True stress controlled fatigue life experiments for elastomers

Kubat Narynbek Ulu, Bertrand Huneau, Erwan Verron, Anne-Sophie Béranger, Patrick Heuillet

True Stress Controlled Fatigue Life Experiments for Elastomers

K. Narynbek Ulu[1,2], B. Huneau[1], E. Verron[1], A.-S. Béranger[2], and P. Heuillet[2]

[1]Ecole Centrale de Nantes, Institut de Recherche en Génie Civil et Mécanique (GeM), UMR CNRS 6183, Nantes, France

[2]LRCCP, Vitry-sur-Seine, France

Abstract

As of present, fatigue life testing of elastomers in displacement control is extensively utilized in academic research and industry. However, there are limitations to this approach, if the tested elastomer behaves inelastically; it can be shown that the mechanical state parameters of the material, stress or strain, do not remain constant throughout the duration of an experiment carried out in displacement control. As such, application of various fatigue criteria is questionable and, moreover, a valid comparison of fatigue resistance of different materials cannot be carried out. In the present work, a procedure is developed that allows uniaxial fatigue life testing in true stress control and creation of the corresponding Wöhler curve. The procedure allows testing of single specimens and is then extended for several specimens in parallel. The procedure is validated by experiments on a synthetic rubber HNBR for three loading levels of true stress amplitude at a loading ratio R=0. The results confirm the viability of the procedure for both individual and parallel testing.

Keywords: fatigue test methods, experimental techniques, rubber, Wöhler curve, S-N curve.

Corresponding author: Bertrand Huneau - *bertrand.huneau@ec-nantes.fr, Tel: +33 2 40 37 68 82, Fax: +33 2 40 37 25 66*

Nomenclature

$.^{\max}$	a maximum value of a parameter during a cycle
$.^{\min}$	a minimum value of a parameter during a cycle
$\Delta\sigma$	true stress amplitude
$\dot{\bar{\sigma}}$	average stress rate
$\dot{\sigma}$	instantaneous stress rate
λ	stretch ratio
σ	true stress
F	force
i	cycle number
l	length in deformed state
l_0	reference length in unstressed state
N_f	fatigue life
R	loading ratio
S	deformed cross-section area of a specimen
S_0	original cross-section area of a specimen
u	displacement
W	strain energy density
DIC	digital image correlation
HNBR	hydrogenated nitrile butadiene rubber
SIC	strain-induced crystallization

1 Introduction

Elastomers have been in extensive use for well over a century. The versatility of elastomeric materials is attributed to their ability to withstand large strain in mostly elastic manner. Both natural and synthetic, they are used in a wide variety of applications (such as tires, hoses, seals, vibration dampeners, etc.) and in many industries (automotive, aerospace, civil, energy, etc.). One of the principal modes of failure of industrial elastomeric products is fatigue, i.e. the material is weakened when it is subjected to long-term cyclic service loading conditions. This failure process is characterized by initiation of cracks and their subsequent growth. Thus, fatigue analysis of elastomers can be investigated by two complementary approaches: fatigue crack propagation and fatigue life [1]. The present work focuses on fatigue life testing, which characterizes crack initiation and growth. Fatigue life results are analyzed within the framework of continuum mechanics, where a history of loading is used for fatigue life prediction; fatigue life itself is defined as the number of cycles until formation of a crack of a specific size or failure of a specimen. It should be noted that fatigue life experiments require testing of a statistically significant number of specimens as there is always some variance (scattering) of the results mainly due to material defects introduced during processing [2]. Finally, there are two fatigue life testing approaches for engineering materials. For the first approach, the goal is to apply a specific stress loading history. In practice, such test are carried out by controlling the force prescribed on the specimen, from which the stress is subsequently calculated. This approach is more suitable for rigid materials such as metals or composites, in which strain to be measured are small. The second approach consists in trying to apply a specific strain loading history; conventionally, experiments are then carried out in displacement control and, as such, this approach is more suitable for flexible materials such as elastomers, because of large deformations. Consequently, fatigue life testing in displacement control is widely utilized for elastomers within industry and in academic research, and there are international standards, *e.g.* [3].

However, it becomes apparent that standardization of fatigue life results and their interpretation, as done for metals, is difficult mainly because of complex behavior of elastomeric materials. The validity of displacement control testing is primarily based on the assumption of elastic response of elastomers, which is not always the case. Hence, experimenters are forced to adopt several major assumptions to overcome the obstacles

faced in fatigue life testing. These issues are discussed in greater detail in the following section. In response, a testing procedure that is based on control of true stress is developed in the present work. First, limitations of the conventional testing procedures are outlined, and a complete experimental procedure is subsequently provided, where fatigue life tests are driven in true stress. The procedure maintains a constant true stress amplitude, $\Delta\sigma = \sigma^{\max} - \sigma^{\min}$ and a constant loading ratio, $R = \sigma^{\min}/\sigma^{\max}$, and maintains them throughout the duration of uniaxial fatigue life experiments; the importance being that these two test parameters fully describe the applied loading condition in terms of mechanical state parameters. Simultaneously with controlling true stress, the developed procedure must be inexpensive in terms of machine time and allow testing of a large number of specimens for statistical significance; moreover, the procedure is to be carried out on specimens of relative simple geometry with future extension to industrial parts with a use of fatigue failure criteria. In addition to that, we believe that testing in true stress control eliminates the many obstacles encountered during conventional testing in displacement control. It is important to note that true stress is the determining factor behind the fatigue phenomenon; it is a mechanical state parameter that is inherent only to the behavior of the material. Correspondingly, a relevant *S-N* (true stress vs. number of cycles) curve, such as the one originally proposed by Wöhler [4], can be produced as a result and a valid interpretation of the results can be achieved, thus allowing comparison between different elastomeric materials upon application of fatigue failure criteria.

2 Limitations of Conventional Testing Procedures

First, the theoretical background for fatigue life testing of elastomers is reviewed and, in the subsequent sections, the limitations of conventional testing procedures are presented.

2.1 Theoretical background

As mentioned previously, the two approaches for fatigue life testing aim to control the applied loading either in terms of strain or stress. At this point, it is important to make a distinction, with respect to experimental practice, between what one can refer to as experimental and mechanical state parameters. The two important experimental parameters are displacement (u) and force (F), and they are related to both material

properties and specimen geometry; with one of the experimental parameters prescribed, the other is measured. On the other hand, strain and true (Cauchy) stress (σ) are the two corresponding mechanical parameters that are inherent only to the material itself; more specifically, the true stress is what is experienced by the material. The mechanical parameters are deduced from post-treatment of experimental parameters. Strain can be represented as the stretch ratio λ. For example in case of simple uniaxial loading, $\lambda = l/l_0$, where l and l_0 are, respectively, the lengths in deformed state and unstressed states (i.e. applied force equals to zero); the former is a function of the applied displacement, $l = l_0+u$. Correspondingly, true stress is defined as $\sigma = F/S$, where F is the applied force and S is the actual cross-section area.

For example, in fatigue life testing of metals, force is prescribed and then stress can be measured, which is used as the main mechanical parameter that determines fatigue life. Engineering stress is commonly used and can be calculated as F/S_0, where S_0 is the initial cross-section area; the rigidity of metals allows to make an equivalence between true and engineering stress within the small strain assumption ($\sigma = F/S \approx F/S_0$). The study of fatigue in metals is extensive: for a given metal, one can find in databases $S-N$ curves; the analysis is then mostly straightforward due to a presence of a wide variety of fatigue initiation criteria based on stress parameters [5, 6].

On the other hand, fatigue life testing of elastomers presents some complications and, unfortunately, is not at the same stage of development. The first studies on natural rubber by Cadwell *et al.* [7] and on synthetic rubber by Fielding [8] utilized maximum principal strain as the tested mechanical state parameter (with combination of minimum strain, mean strain, strain amplitude, or the loading ratio). Another strain-based mechanical state parameter has been also used in a form of strain energy density, a mechanical state parameter [9]; several fatigue life criteria have been developed [10, 11, 12]. The principal advantages of this parameter are in its application to multiaxial loading. For both strain based approaches, the $S-N$ curve is often replaced by $\lambda-N$ or $W-N$ curves for principal strain and strain energy respectively.

2.2 Inelastic response of elastomers and its effect on testing

Control of displacement, an experimental parameter, is utilized in common practice for the strain-based approaches. Afterwards, the mechanical parameters are calculated from

the prescribed displacement and measured force: calculation of maximum principal strain from the prescribed displacement; similarly, strain energy release rate from displacement and force, or estimated by finite element analysis. The principal underlying assumption of these strain-based approaches is the mostly elastic response of elastomers. That is, provided with a constitutive equation for a specific material, one can determine the mechanical parameters experienced by a material for any prescribed or measured experimental parameters. In reality, one encounters several hurdles in fatigue life testing of elastomers when their response is not completely elastic. In this case, determination of the mechanical parameters from the experimental ones is considerably more difficult than for metals [13].

Primarily, the behavior of filled rubbers includes many complex phenomena where interactions between them are not well understood; these phenomena can be described as dissipative mechanical responses that emerge as hysteresis on a stress-strain curve of an elastomeric material [14, 15, 16]. During cyclic loading of a filled virgin material, significant softening can be observed during cyclic loading for several initial cycles; this large-strain hysteresis mechanism is referred to as the Mullins effect [17]; Figure 1 shows

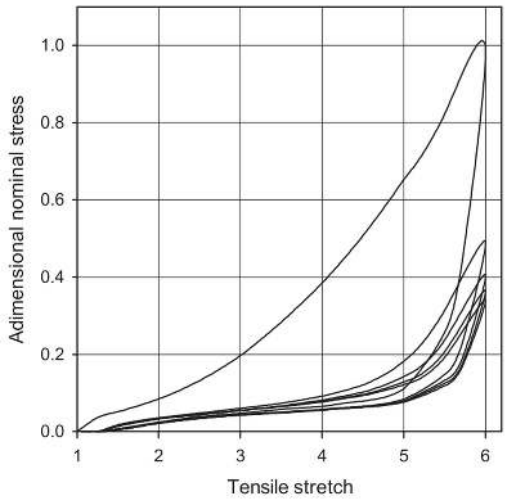

Figure 1: Experimental example of the Mullins effect. Taken with authors' permission from [18].

an experimental example of the Mullins effect, where after each successive cycle, the stress decreases for the same strain level. The Mullins effect can reappear after the initial cycles, if the material is subjected to a higher and new maximum loading. In addition to stress softening, inelastic strain is observed after each successive unloading. In Figure 1, the measured strain does not equal to zero in an unstressed state (F or σ=0); therefore in practice, a compressive force for massive specimens or buckling for thin specimens at zero

displacement is observed.

After this softening during the first cycles, further decrease in measured stiffness is continued to be observed under cyclic loading at constant displacement amplitude. It also manifests as accumulation of inelastic strain during loading and/or in an unstressed state; this softening is classically attributed to the viscoelastic nature of elastomers. In literature, this phenomenon is referred to as "cyclic stress relaxation" (and as "cyclic creep" or "ratcheting" for tests carried out in force control) [19, 20, 21, 22, 23, 24]; hereinafter, this phenomenon is referred to as *long-term cyclic stress relaxation* (or for brevity as *long-term relaxation*) since its effects are only evident after a large number of cycles.

The two relaxation behaviors are present in all elastomers. However, the degree to which the two behaviors affect fatigue life testing of elastomers varies depending on the material. For some elastomers, the Mullins effect is present (for filled formulations) and the second softening phenomenon can be sometimes considered as negligible; conventional testing approaches appear to be viable in this case, but with some drawbacks. For some others, both relaxation phenomena are significant and cannot be ignored during fatigue life testing. These two ideal cases are expanded hereinafter.

2.2.1 Case 1 - Mullins effect with insignificant long-term cyclic stress relaxation

Considerable experimental work has been carried out on fatigue life of filled NR, which exhibits mostly elastic behavior. The Mullins effect is present; however in general, after a relatively small number of cycles, the stress-strain curve is assumed to somewhat stabilize and overlap on each successive cycle (i.e. there is no significant long-term cyclic stress relaxation). Thus, when NR is tested in displacement control, it is assumed that the displacement-strain relationship does not change and the stress-strain relationship stabilizes after some cycles and enters a *plateau* region [1, 3, 25, 22, 26, 27]. It appears that transition to this phase is highly dependent on the material, its composition, specimen geometry, *etc.* For example, André *et al.* [28] carried out uniaxial and biaxial experiments in displacement control for NR. Since the tested material exhibited negligible viscoelastic response and the force seemed to stabilize after 100 cycles, authors used a generalized Mooney Rivlin model to calculate the true stress by finite element analysis and plot the

results in terms of that mechanical parameter. Overall, there is no consensus on the best approach for this *accommodation* for the Mullins effect, which makes comparison between different studies somewhat problematic. There exists a wide variety of academic and industrial testing protocols, which try to take into account the Mullins effect exhibited by the material before the actual fatigue life testing. The common differences arise in the number of cycles to accommodate for the Mullins effect or in the level of loading at which the accommodation is to be performed (as the Mullins effect is highly dependent on the maximum loading level previously experienced by the material). Moreover, the accommodation is entirely absent in some studies [29, 30, 31, 32].

Another consequence of the Mullins effect, which is largely not acknowledged, is on the R-ratio. As mentioned earlier, a specimen is in compression at zero displacement after the initial cycles; if one requires an R-ratio of zero and applies a displacement loading with a R-ratio of zero for example ($R = u^{\min}/u^{\max}$), the actual R-ratio in terms of strain ($R = (\lambda^{\min} - 1)/(\lambda^{\max} - 1)$) and stress ($R = \sigma^{\min}/\sigma^{\max}$) will be negative as the minimum stretch ratio, $\lambda^{\min}$, is less than one and the minimum stress, $\sigma^{\min}$, is also negative; thus, the real, mechanical R-ratio values are smaller that the experimental one in terms of displacement. The R-ratio is important in fatigue testing of elastomers, especially in cases of presence of strain-induced crystallization (SIC) [33, 34]. In general, increased presence of SIC improves fatigue resistance of elastomers as numerous studies have shown that the incidence of SIC is sensitive to the R-ratio [16, 28, 32, 35].

Finally, it is common to find experiments carried out in displacement control and a *pseudo*-Wöhler curve to be plotted with calculated engineering stress, determined after a certain number of cycles or averaged over the duration of the experiment [32, 36]. However, engineering stress is not a good representative of the mechanical state of the material under loading due to large strain and inelastic behaviors [37]. To summarize, the main problem with this approach is that many fatigue life testing protocols exist, but these are not equivalent; interpretation of different studies and comparison of different elastomers is complex at best and erroneous at worst.

In order to describe the evolution of experimental and mechanical parameters for a material exhibiting such behavior, we present a straightforward thought experiment with equations of a specimen tested under cyclic uniaxial loading in displacement control. We divide this particular case into two phases: first of the Mullins effect and second of sta-

bilized stress-strain behavior. With reference to Figure 1, Figure 2 presents a simplified

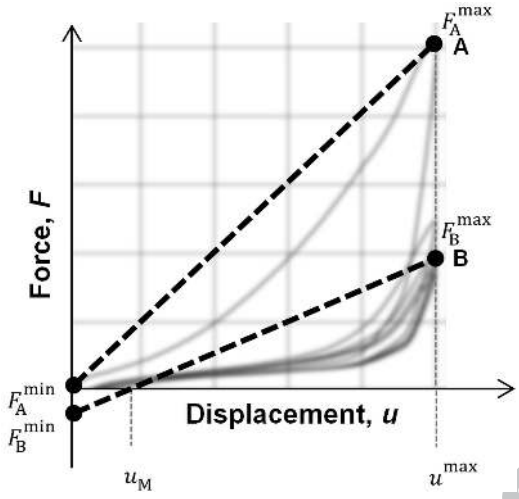

Figure 2: Case 1 - Simplified representation of the Mullins effect with insignificant long-term cyclic stress relaxation.

representation of the loading paths at: cycle A - the first loading cycle; and cycle B - sometime after the initial cycles, when the behavior of the material stabilizes. Displacement loading is from zero to $u^{\max}$. At both A and B, we can measure the maximum and minimum forces, $F^{\max}$ and $F^{\min}$ respectively. During cycle B, due to stress softening, the specimen is in compression at zero displacement; and there is inelastic strain due to stress softening: displacement u_{M} (M for Mullins) does not equal to zero when force is equal to zero. The maximum strain at $u^{\max}$ after loading A is:

$$\lambda_{\mathrm{A}}^{\max} = \frac{l_0 + u^{\max}}{l_0} = \frac{l_{\max}}{l_0}, \tag{1}$$

However at B, the reference length is no longer l_0, but $l_0 + u_{\mathrm{M}}$. Thus, the maximum strain at B equals to:

$$\lambda_{\mathrm{B}}^{\max} = \frac{l_{\max}}{l_0 + u_{\mathrm{M}}} = \frac{l_{\max}}{l_0} + \frac{l_0}{l_0 + u_{\mathrm{M}}} = \frac{\lambda_{\mathrm{A}}^{\max}}{\lambda_{\mathrm{M}}}, \tag{2}$$

where λ_{M} is the reference strain at B with respect to the original specimen length. Therefore, we can conclude that:

$$\lambda_{\mathrm{B}}^{\max} < \lambda_{\mathrm{A}}^{\max}. \tag{3}$$

To calculate the true stress at $u^{\max}$, first the cross-section area needs to be known. Assuming incompressibility, $S = S_0/\lambda$ and thus the cross-section area at A equals to:

$$S_{\mathrm{A}}^{\max} = \frac{S_0}{\lambda_{\mathrm{A}}^{\max}}. \tag{4}$$

However at B, the original area is not S_0 anymore, but S_0/λ_{M} due to the inelastic strain and, thus, the area is:

$$S_{\mathrm{B}}^{\max} = \frac{S_0/\lambda_{\mathrm{M}}}{\lambda_{\mathrm{B}}^{\max}}. \tag{5}$$

From Eq. 2, it leads to:

$$S_{\mathrm{B}}^{\max} = \frac{S_0}{\lambda_{\mathrm{A}}^{\max}} = S_{\mathrm{A}}^{\max}. \tag{6}$$

Finally, the maximum and minimum stresses can be calculated at A:

$$\sigma_{\mathrm{A}}^{\max} = \frac{F_{\mathrm{A}}^{\max}}{S_{\mathrm{A}}^{\max}}, \tag{7}$$

$$\sigma_{\mathrm{A}}^{\min} = \frac{F_{\mathrm{A}}^{\min}}{S_0} = 0. \tag{8}$$

In similar fashion, we can deduce that the maximum and minimum stress at B are respectively smaller than at A:

$$\sigma_{\mathrm{B}}^{\max} = \frac{F_{\mathrm{B}}^{\max}}{S_{\mathrm{B}}^{\max}} = \frac{F_{\mathrm{B}}^{\max}}{S_{\mathrm{A}}^{\max}} < \sigma_{\mathrm{A}}^{\max}, \tag{9}$$

$$\sigma_{\mathrm{B}}^{\min} = \frac{F_{\mathrm{B}}^{\min}}{S_0} < \sigma_{\mathrm{A}}^{\min}. \tag{10}$$

Thus, Figure 3 summarizes the above in a simplified schematic with the evolution of the

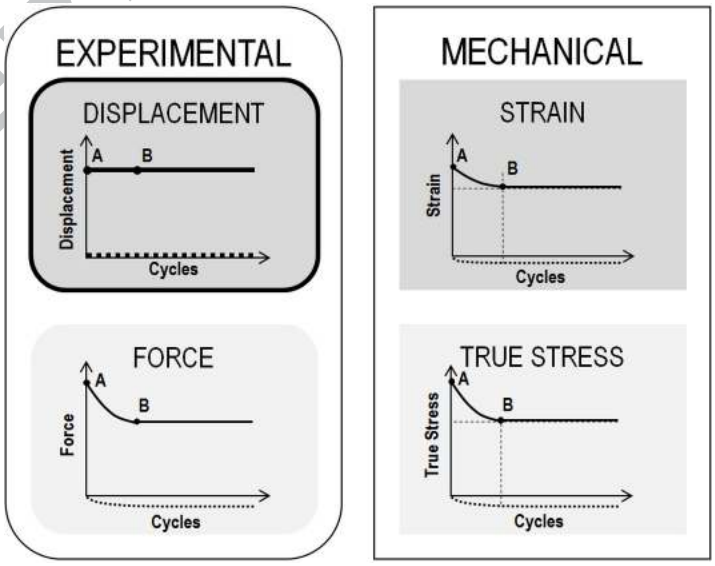

Figure 3: Case 1 - Mullins effect with insignificant long-term cyclic stress relaxation; evolution of force, strain, and true stress under constant cyclic loading in displacement control (bold outline).

two experimental parameters, displacement and force, and the two mechanical parameters, strain and stress. After point B, both mechanical parameters are relatively constant and

the material can be said to enter the *plateau* region as indicated by the dashed lines. A relationship between the prescribed displacement and the strain can be established; consequently, a hyperelastic model can be used to calculate true stress. For natural rubber, these assumptions appear somewhat reasonable; for example, fatigue life tests carried out separately in displacement control and force control have comparable fatigue lives for equivalent strain and stress loading, if the testing is carried out under identical experimental conditions (material formulation, accommodation procedure, temperature, specimen geometry, *etc.*) [38]; however, Royo [39] reports that for some other elastomers (type not reported) the ranking of fatigue resistances is inconsistent depending on load or force control. And as mentioned earlier, the real R-ratio, either in terms of stress or strain, is smaller in this particular case. Finally, it should be noted again that not a single elastomeric material exhibits such idealized behavior; as one of the many experimental variables change, analysis of results becomes complicated.

2.2.2 Case 2 - Mullins effect with long-term cyclic stress relaxation

On the other hand, it appears that use of displacement control proves to be unsatisfactory, if the elastomeric material exhibits significant long-term inelastic behavior. We can extend the previous deductions for an additional third phase, where there is continuous cyclic stress relaxation after the Mullins effect. Figure 4 shows a cycle, C, that occurs some time

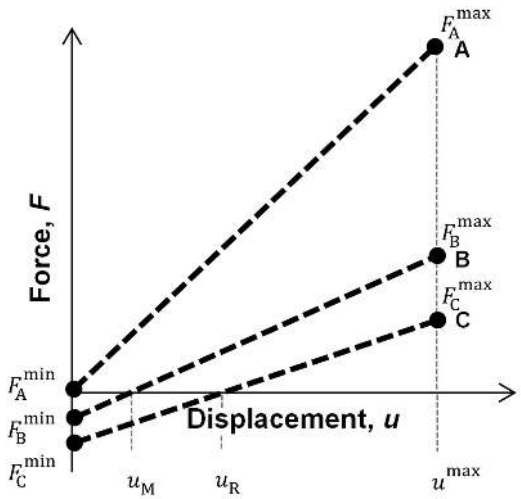

Figure 4: Case 2 - Simplified representation of the Mullins effect with long-term cyclic stress relaxation.

long after cycle B, and represents a long-term continuous decrease in measured maximum and minimum forces in addition to inelastic strain, which is evident from the distance u_R.

Similar to Eq. 2, the maximum strain at C is:

$$\lambda_{\mathrm{C}}^{\max} = \frac{l_{\max}}{l_0 + u_{\mathrm{R}}} = \frac{\lambda_{\mathrm{A}}^{\max}}{\lambda_{\mathrm{R}}} < \lambda_{\mathrm{B}}^{\max} < \lambda_{\mathrm{A}}^{\max}. \tag{11}$$

The cross-section area at $u^{\max}$ also remains constant:

$$S_{\mathrm{C}}^{\max} = \frac{S_0/\lambda_{\mathrm{R}}}{\lambda_{\mathrm{C}}^{\max}} = \frac{S_0}{\lambda_{\mathrm{A}}^{\max}} = S_{\mathrm{A}}^{\max}, \tag{12}$$

and the maximum and minimum stress decrease with respect to B and A:

$$\sigma_{\mathrm{C}}^{\max} = \frac{F_{\mathrm{C}}^{\max}}{S_{\mathrm{C}}^{\max}} = \frac{F_{\mathrm{C}}^{\max}}{S_{\mathrm{A}}^{\max}} < \sigma_{\mathrm{B}}^{\max} < \sigma_{\mathrm{A}}^{\max}, \tag{13}$$

$$\sigma_{\mathrm{C}}^{\min} = \frac{F_{\mathrm{C}}^{\min}}{S_0} < \sigma_{\mathrm{B}}^{\min} < \sigma_{\mathrm{A}}^{\min}. \tag{14}$$

Moreover, if such material is tested in force control, there is presence of long-term cyclic creep that is equivalent to long-term relaxation; we can make similar observations as shown in Figure 5. The strain at A for $F^{\max}$ is:

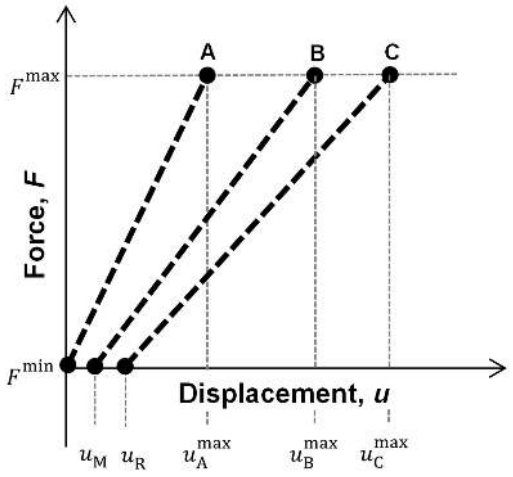

Figure 5: Case 2 - Simplified representation of the Mullins effect with long-term cyclic creep.

$$\lambda_{\mathrm{A}}^{\max} = \frac{l_0 + u_{\mathrm{A}}^{\max}}{l_0}, \tag{15}$$

At B and C, the strain are slightly different:

$$\lambda_{\mathrm{B}}^{\max} = \frac{l_0 + u_{\mathrm{B}}^{\max}}{l_0 + u_{\mathrm{M}}}, \tag{16}$$

$$\lambda_{\mathrm{C}}^{\max} = \frac{l_0 + u_{\mathrm{C}}^{\max}}{l_0 + u_{\mathrm{R}}}. \tag{17}$$

Without experimentation, it is impossible to tell whether there is or to what extent strain changes from A to C; there is no direct relationship between u_{M}, u_{R}, $u_{\mathrm{A}}^{\max}$, $u_{\mathrm{B}}^{\max}$, and $u_{\mathrm{C}}^{\max}$. It is possible that strain remains constant if the condition $\frac{l_0+u_{\mathrm{A}}^{\max}}{l_0} = \frac{l_0+u_{\mathrm{B}}^{\max}}{l_0+u_{\mathrm{M}}} = \frac{l_0+u_{\mathrm{C}}^{\max}}{l_0+u_{\mathrm{R}}}$ is satisfied. However, it does not seem probable that all the different experimental parameters lead to such equivalence. Nevertheless, as a remark, it could be shown that the strain could be constant from A to C only under one condition, where the general relationship between maximum and minimum displacements satisfies:

$$\frac{u^{\max} + l_0}{u^{\min} + l_0} = constant. \tag{18}$$

If we extend these deductions to the surface area, it is clear that the cross-section area at $F^{\max}$ decreases from A to C. Since at A it equals to:

$$S_{\mathrm{A}}^{\max} = \frac{S_0}{\lambda_{\mathrm{A}}^{\max}}, \tag{19}$$

but at B, the surface area is:

$$S_{\mathrm{B}}^{\max} = \frac{S_0/\lambda_{\mathrm{M}}}{\lambda_{\mathrm{B}}^{\max}} = \frac{S_0}{\lambda_{\mathrm{M}}\lambda_{\mathrm{B}}^{\max}}. \tag{20}$$

One can show using Eq. 15 and Eq. 16 that $S_{\mathrm{A}}^{\max}$ is greater than $S_{\mathrm{B}}^{\max}$ due to the relationship between the denominators of Eq. 19 and Eq 20:

$$\lambda_{\mathrm{M}}\lambda_{\mathrm{B}}^{\max} = \left(\frac{l_0 + u_{\mathrm{M}}}{l_0}\right)\left(\frac{l_0 + u_{\mathrm{B}}^{\max}}{l_0 + u_{\mathrm{M}}}\right) = 1 + \frac{u_{\mathrm{B}}^{\max}}{l_0} > 1 + \frac{u_{\mathrm{A}}^{\max}}{l_0} \equiv \lambda_{\mathrm{A}}^{\max}. \tag{21}$$

Similar reasoning can be extended to point C to show that $S_{\mathrm{A}}^{\max} > S_{\mathrm{B}}^{\max} > S_{\mathrm{C}}^{\max}$. So finally, given that the applied force is constant, the maximum true stress ($\sigma = F/S$) increases from A to C.

Finally, it can be concluded that due to long-term stress relaxation, application of procedures based on displacement control (Figure 6) or force control (Figure 7) is not valid given the fact that both mechanical parameters experienced by the material, strain and stress, appear to be never constant throughout the duration of the experiment; there is no stabilization of the stress-strain behavior. Hence, proper analysis of the fatigue

life results is not possible and the results obtained are not valid for such materials. To overcome these limitations, a procedure in true stress control is developed as presented in the next section.

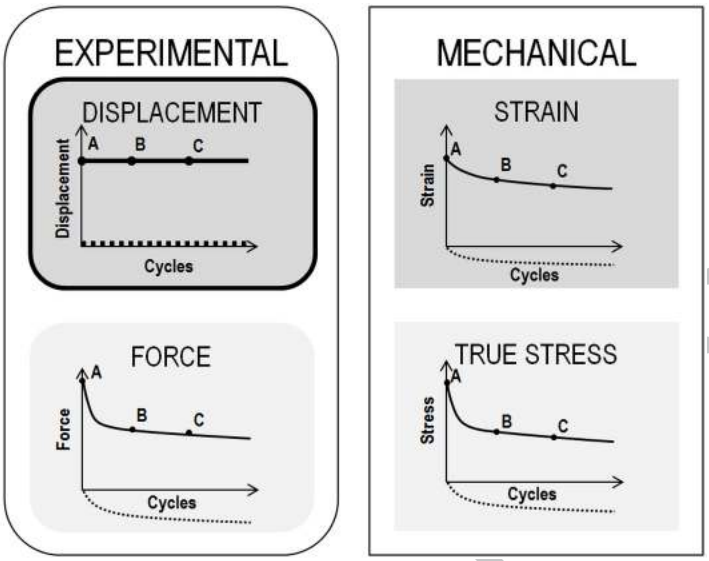

Figure 6: Case 2 - Mullins effect with long-term cyclic stress relaxation; evolution of force, strain, and true stress under constant cyclic loading in displacement control (bold outline).

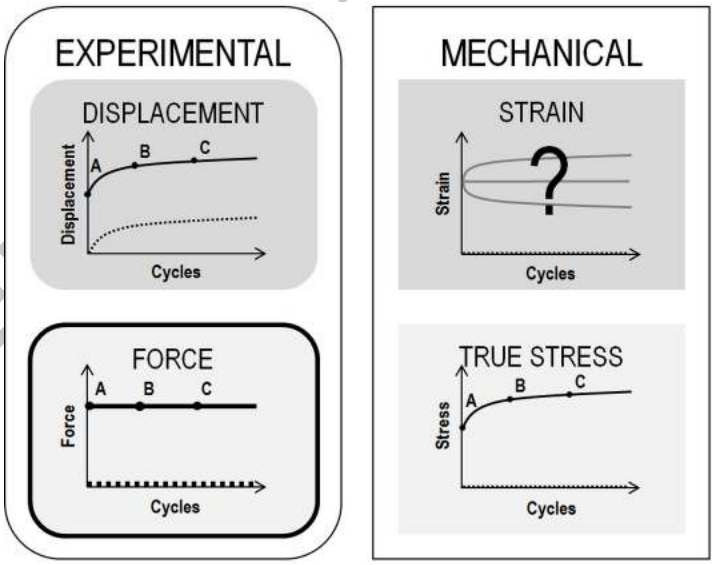

Figure 7: Case 2 - Mullins effect with long-term cyclic creep; evolution of displacement and true stress under constant cyclic loading in force control (bold outline).

3 Development of a "True Stress" Control Procedure

Testing elastomers in true stress control has been reported for biaxial loading [40], but it remains little used primarily due to complexity of maintaining true stress over the duration of the experiment. However, it is one way to alleviate the problems associated with the conventional testing procedures. True stress control permits to keep at least one of the mechanical state parameters constant throughout the duration of the experiment. Thus, the Mullins effect or long-term stress relaxation are naturally taken into account, because stress itself is controlled. Thus, the objective of the present procedure is to control the true stress amplitude for a given loading ratio, R:

$$\Delta\sigma = \sigma^{\max} - \sigma^{\min}, \tag{22}$$

during uniaxial cyclic loading of a specimen, where $\sigma^{\max,i} = \mathrm{Max}(F/S)$ and $\sigma^{\min,i} = \mathrm{Min}(F/S)$ for each cycle i; F being the real-time force measured by a machine load-cell and S being the real cross-section area in the gauge-length of the specimen. The procedure is split into two parts: first, the procedure for testing on a single specimen is presented; and then it is expanded for testing of multiple specimens in parallel.

3.1 Procedure for testing of individual specimens

3.1.1 Calculation/determination of cross-section area

The initial step consists in calculating the cross-section area of the specimen *a priori* as a function of imposed displacement. Initially, DIC measurements are performed on a sample at specific cycle intervals (*e.g.* every thousand cycles) to measure the cross-section area as a function of prescribed displacement $S(u)$. A sinusoidal waveform in displacement control is applied with a loading ratio $R = 0$. Assuming that the material is isotropic, transverse strain λ_2 is measured for different values of the maximum displacement and it can be deduced that $\lambda_2 = \lambda_3$; for anisotropic materials, it is necessary to measure both λ_2 and λ_3. Afterwards, the cross-section area can be calculated from the initial dimensions of the specimen. The DIC measurements can be supplemented by finite element analysis. The methodologies for finite element analysis are outside the scope of the present work,

but special care should be taken to properly take into account hyperelastic, viscoelastic, and/or plastic/viscoplastic behaviors of the material under cyclic loading.

3.1.2 Machine control algorithm

The next step is the live machine control algorithm. The goal is to prescribe the displacement of the machine actuator to maintain a constant true stress amplitude target. The algorithm is run for simultaneous control of minimum and maximum true stress as seen in Figure 8. It should be noted that the algorithm is cyclic dependent and independent of the utilized testing frequency. After the target stress values are set, the real-time readings

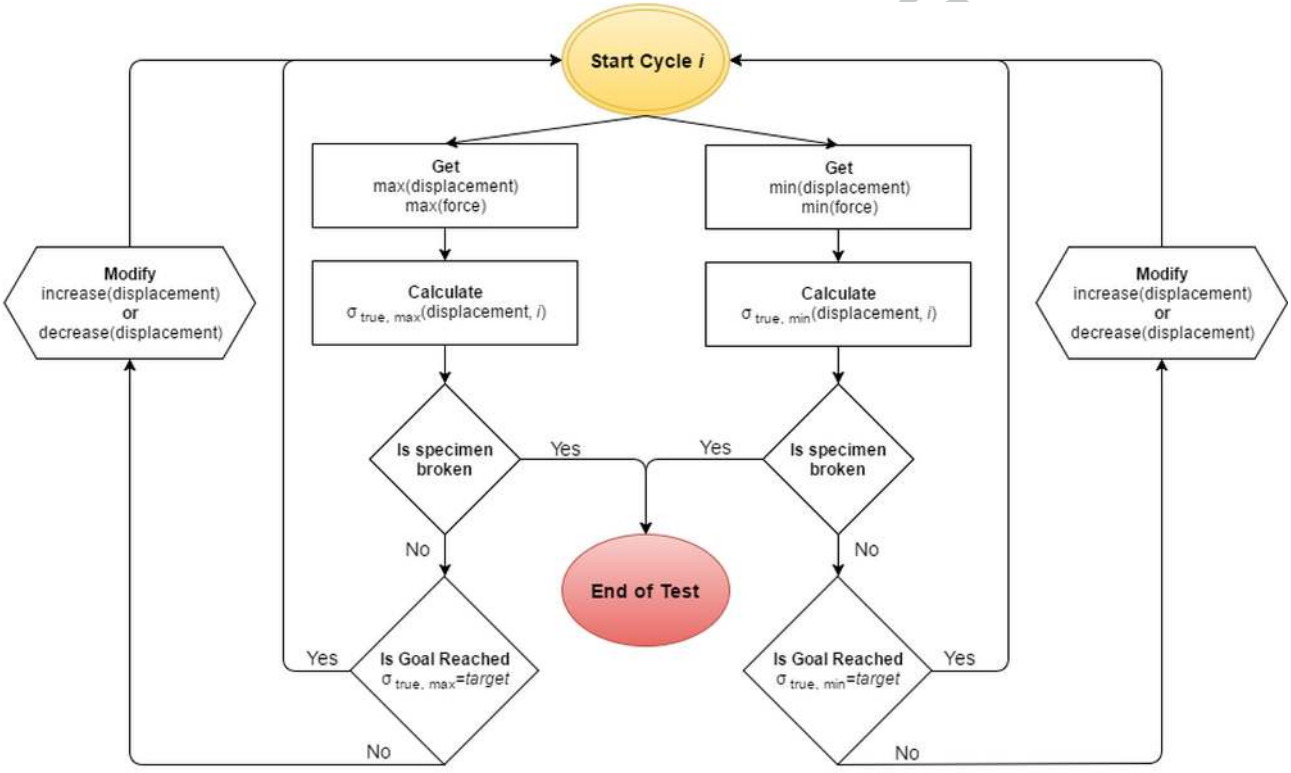

Figure 8: Machine control algorithm.

of force and displacement are taken at each cycle from the machine. Then the true stress amplitude is calculated by Eq. 22; maximum and minimum true stress at each cycle are calculated respectively by:

$$\sigma^{\max,\mathrm{i}} = \mathrm{Max}\left(\frac{F(t)}{S(u(t))}\right), \tag{23}$$

and

$$\sigma^{\min,\mathrm{i}} = \mathrm{Min}\left(\frac{F(t)}{S(u(t))}\right) \tag{24}$$

where t is the time elapsed for each cycle i. Afterwards, the algorithm checks at each cycle whether the specimen has broken (by monitoring measured force with respect to prescribed

displacement) and the test is terminated in such case. If the specimen is still intact, the actual true stress amplitude is compared with the target; depending on the value of the actual minimum and maximum true stress values, the prescribed displacement (maximum and minimum values) is corrected (increased or decreased) in small increments. The magnitude of displacement increments controls how fast the machine control algorithm can achieve the desired true stress loading: if too small, the number of cycles to reach the target stress could be too long and would interfere with fatigue results; a large increment could cause an overshoot of the maximum or minimum target stress, which is not desired in fatigue testing as it can negatively influence the results by damaging the material. It should be noted that the increment magnitude is highly dependent on the material, specimen geometry, and the testing machine itself. Afterwards, the next cycle is run under the newly modified displacement values and the procedure iterates. In practical terms, the utilized experimental setup must have the following basic requirements. The first is the ability to monitor and control the displacement of the testing machine actuator continuously and in real-time. Second, the experimental setup must be equipped with a load-cell (of sufficient accuracy for dynamic loading), from which one can export the measurements into the algorithm. Finally, the algorithm itself is to be implemented in a controller, which is usually included with the testing machine or as a personal computer of sufficient processing power. For such experimental setup, the main limitation appears to be an ability to impose displacement in real-time. A setup can be custom-built, but several commercial solutions (by major fatigue testing equipment manufacturers) have been encountered that possess this functionality.

3.2 Expansion of the procedure for testing of multiple specimens

As noted earlier, fatigue life testing often requires testing of a large number of specimens due to scattering of results. Therefore, it is often valuable to be able to test several specimens in parallel as to minimize the machine time and the overall testing time. The machine control algorithm can control true stress loading only on one specimen and cannot be extended to testing of specimens in parallel. Such algorithm cannot take into account presence of large cracks or complete breaks of one or more specimens tested in parallel, because the effective surface area of all specimens in parallel drastically changes. Thus,

true stress control is not theoretically possible (with a single machine actuator) upon extension to parallel testing.

This limitation is overcome by creating master displacement curves that correspond to a specific true stress loading. The master displacement curves contain minimum and maximum prescribed displacement values at each cycle over duration of an experiment for a specific loading level. Such approach ensures that when the effective surface area changes, the stress experienced by other specimens remains constant. To create the master curves, the displacement values for each cycle are derived from the experiments run on single specimens at desired true stress targets as specified in Section 3.1 (i.e. preliminary individual testing is required *a priori* and real-time adjustments are not done during parallel testing). At each cycle, positions of the machine actuator corresponding to maximum and minimum displacements are recorded, which in the end serve as references for the master curves. Variation of individual specimen dimensions, processing defects of the material (internal voids, heterogeneity of the material), and other unforeseen variables could affect the displacement prescribed for each individual specimen for the same true stress target. Therefore, it is important to test several specimens under the desired loading conditions to verify that these variables do not have a significant effect. In practice, a basic experimental setup must consist of specimen grips in parallel and of an apparatus to detect failure of each specimen (for example a camera). However, ideally, the authors insist on employing individual force sensors for each specimen grip (such setup is used in the present work and is described in the next section); this allows to monitor loading on each specimen and also detect specimen failure (or any other failure criteria). At this point it should be noted that applying an exact true stress load on all specimens in parallel is challenging. Experimental variables and conditions are always present that will cause the true stress experienced by each specimen to be different (introducing dispersion in stress values in addition to the fatigue life). However, the present procedure allows to approximate the applied true stress load on specimens in parallel. To validate the extension to parallel testing, the true stress experienced by each specimen must be quasi-constant and close to the target.

4 Validation of the Procedure

4.1 Material, specimen, and experimental apparatus

Carbon black filled (70 phr, N772), peroxide cross-linked hydrogenated nitrile butadiene rubber (HNBR) is used for validation of the procedure. This material is chosen as it represents a "worst-case" scenario, where the material exhibits significant Mullins effect and cyclic stress relaxation. Figure 9 shows the fatigue specimen used in the experiments. The gauge length is 10 mm and the stress state is one of uniaxial tension. The specimens are cut using a die from compression molded sheets of the material.

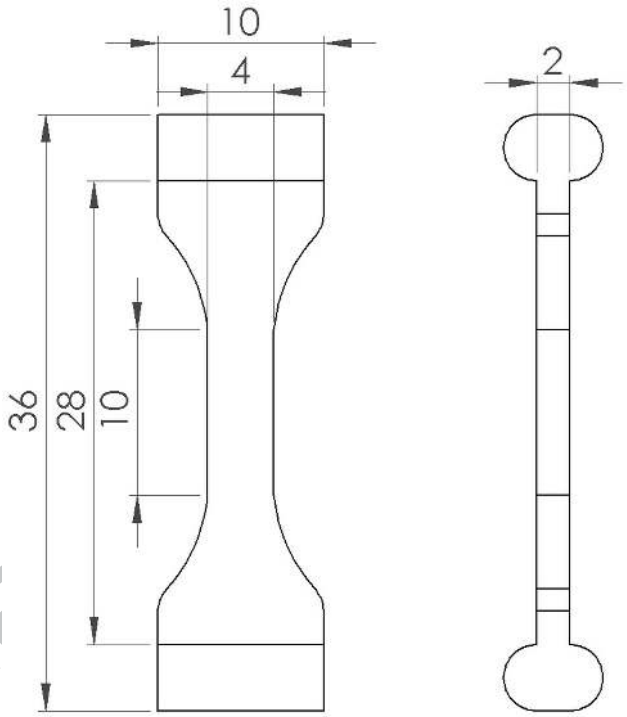

Figure 9: Geometry of specimen.

Testing is performed on an electrically driven machine, *Instron E10000* with a heating chamber set at a temperature so that the surface of the specimen under loading, measured by a pyrometer, is at 120°C (the testing temperature is specific to the service temperature of this grade of HNBR). The machine allows for simultaneous testing of up to 8 specimens in parallel with a use of a custom grip design as shown in Figure 10. Each individual specimen grip is equipped with a force load-cell (*HBM S-Type* 500 N) in order to monitor the fatigue life and the force experienced by each specimen; the design also allows for zeroing of force for each individual specimen. Additionally, a camera is utilized for digital image correlation (DIC) measurements.

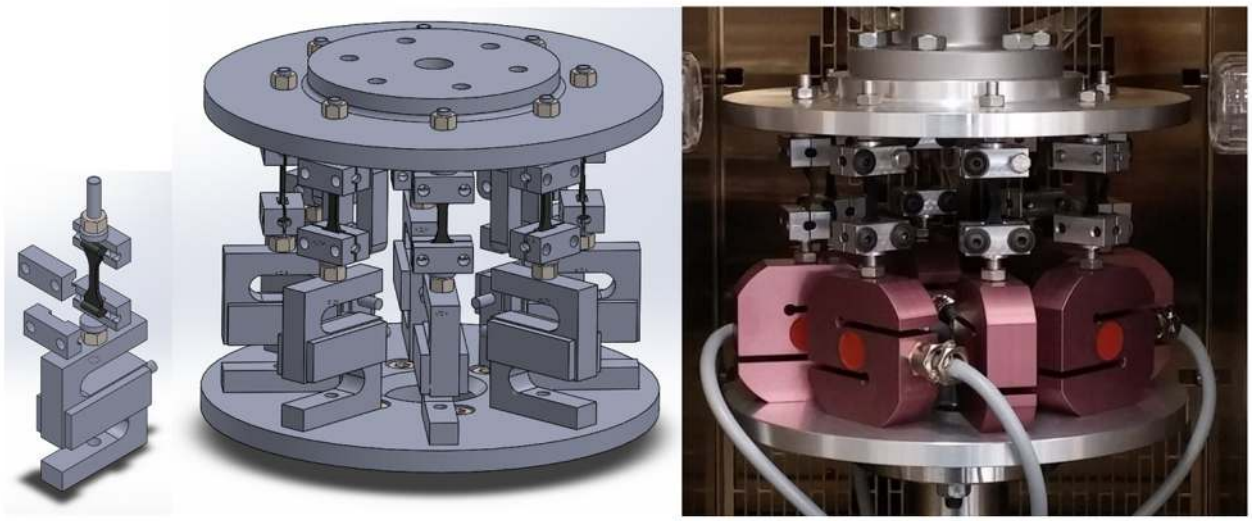

Figure 10: Custom grip design for parallel testing.

4.2 Implementation of the procedure

4.2.1 Calculation of cross-section area

Initially, DIC measurements are made for cyclic tests that are carried out in displacement control. Constant amplitudes of 30 mm, 45 mm, and 55 mm are applied with a loading ratio of R=0 at a frequency of 3 Hz (limitation imposed by camera speed, but within the same order of magnitude as for fatigue life testing). Several cycles are analyzed at 10, 1000, and 10,000 cycles for each amplitude to calculate the evolution of the cross-section area with respect to the prescribed displacement. To confirm the results of DIC measurements, a finite element analysis is also carried out in commercial software *Abaqus* for the given material and geometry. Hyperelastic behavior is modeled by the Arruda-Boyce model [14] with the following coefficients: μ=1.57 MPa, λ_m=2.1, and D=10^{-4} MPa^{-1}; the coefficients are a best-fit of uniaxial tension results. The linear viscoelastic behavior is modeled with a 1-term Prony series and the following coefficient are used: g_1=0.398, k_1=0, and τ_1=0.347. Cyclic loading up to 60 mm is prescribed at a frequency of 3 Hz.

The results of DIC measurements and FE analysis results are presented in Figure 11. From DIC experiments, it is evident that, for the given material, the relationship between the area and the prescribed displacement is constant at least up to 10,000 cycles irrespective of the amplitude. Moreover, there is good correlation between the DIC measurement and FE analysis results. A best-fit polynomial curve of degree 6 is used to approximate

the cross-section area as a function of prescribed displacement. Within the developed algorithm, this polynomial function then calculates the real-time area from real-time displacement readings given by the machine.

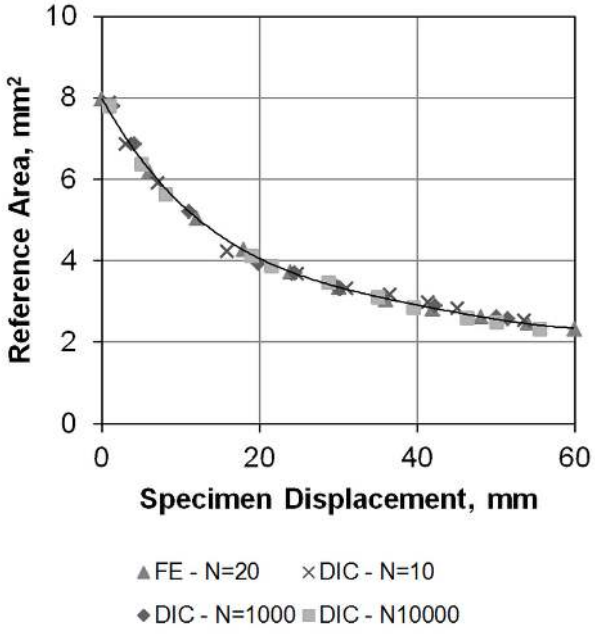

Figure 11: Reference area of the specimen with respect to displacement prescribed by testing machine. Average area is shown for DIC cycles 10, 1000, and 10000 and FE analysis at cycle 20. A polynomial best-fit curve is shown.

4.2.2 Testing individual specimens

The present testing machine software (*Instron WaveMatrix*), allows implementation of a script in *C#* programming language to realize the algorithm presented in Figure 8. It calculates true stress and prescribes a sinusoidal waveform in displacement control. Afterwards, single specimens are tested at R=0 with three loading levels of stress amplitude ($\Delta\sigma$ = 8, 6, and 4 MPa). A constant average stress rate ($\dot{\bar{\sigma}} = [\mathrm{Max}(\sigma) - \mathrm{Min}(\sigma)]/\Delta t$ at each cycle) of 20 MPa/s is used; it should be noted that average stress rate is different from instantaneous stress rate ($\dot{\sigma} = d\sigma/dt$). The reason behind this choice lies in the fact that using a constant frequency is not ideal since the stress rate, which is a mechanical parameter that influences the behavior of the material, is not constant for different loading levels. The nominal frequencies that correspond to constant average stress rate of 20 MPa/s are calculated *a priori* to be 2.5 Hz, 3.33 Hz, and 5 Hz for $\Delta\sigma$ = 8, 6, and 4 MPa, respectively. Due to the nature of the algorithm, it is expected that some number of cycles are required to reach the target true stress amplitude; this number of cycles is omitted from the total fatigue life. Finally, the experiments are stopped at 2 million cycles.

4.2.3 Testing in parallel

For parallel testing, master displacement curves for the three loading levels are created from the tests performed on individual specimens. The minimum number of individually tested specimens is two to three per loading level in order to ensure repeatability. These master curves are derived by calculating the averages at each loading level for both minimum and maximum prescribed displacement values. Due to technical limitations, the maximum and minimum displacements are not recorded for each cycle, but at specific intervals; linear interpolation is used to compute points between recorded values. Moreover, it is assumed that formation of large cracks and their propagation occurs at the end of the fatigue life due to thin geometry of specimens. Consequently, data from the last 10% of cycles ($i \in [90\% * N_f, N_f]$) are omitted in calculation of the master curve; here, it is assumed that cracks might reach a significant size, thereby reducing the real cross-section area and leading to an incorrect calculation of true stress.

Finally, the inherent statistical scattering in fatigue life testing needs to be taken into account at this stage; it implies that the 2-3 tests carried out on individual specimens at each loading level for creation of a master curve, in most cases, do not represent a test with the longest fatigue lifetime. Therefore, the minimum and maximum displacement values need to be extrapolated, if the testing is to undergo for longer duration. In the present study, based on the specific behavior of the material and the specimen geometry, a well-chosen function of best-fit is extrapolated up to 2 million cycles from the last 50% of cycles for both the maximum and the minimum imposed displacements (after initially excluding the final 10% of cycles related to crack propagation, *i.e* best-fit within $i \in [50\% * (90\% * N_f), 90\% * N_f])$.

4.3 Results

4.3.1 Testing individual specimens

The procedure produces consistent results irrespective of the loading level. As an example, Figure 12 shows minimum and maximum displacement prescribed by the testing machine on three different individual specimens in order to reach a constant stress amplitude of $\Delta\sigma$=6 MPa at R=0. First, the target true stress amplitude of 6 MPa is reached for all three specimens. Second, one can identify two phases during stress control. The first phase,

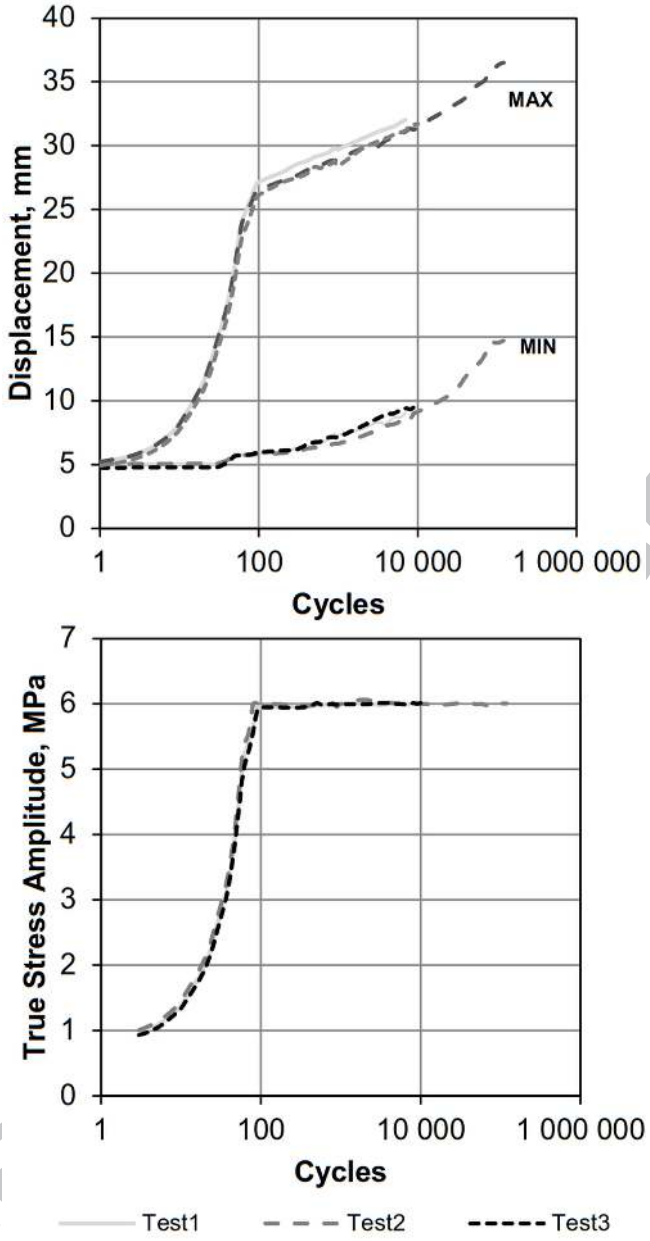

Figure 12: Evolution of maximum and minimum displacements, and true stress amplitude of three separate tests with; target - 6 MPa and R=0.

up to around 100 cycles, is comprised of machine stabilization (the sinusoidal waveform increases gradually in its amplitude to a specified target) and machine stabilization, where the algorithm is reaching the target of 6 MPa. After these 100 cycles, the target stress is reached and both minimum and maximum prescribed displacements stabilize with no significant changes to the amplitude. For other loading levels (4 and 8 MPa), the number of cycles comprising the first phase varies; in general, an assumption is made that this stabilization phase is acceptable, if it takes up less than 2% of the average fatigue life at that loading level. As mentioned earlier, these cycles are not included in the fatigue life. The R-ratio in terms of true stress equals to zero. Additionally, it is important to note

that in Figure 12 all three specimens have different fatigue lives (around 7800, 122400, and 11400 cycles until complete fracture of the specimen). Considering this, the prescribed minimum and maximum displacement have good correlation and repeatability. Hence, one can deduce that a master curve for this specific loading level can be created.

4.3.2 Testing in parallel

Figure 13 shows the master displacement curves derived from the individual tests for the three loading levels. The dashed lines represent the extrapolated maximum and minimum displacement values (as mentioned in Section 4.2.3) and the initial cycles (100 for 8 MPa, 200 for 6 MPa, and 300 for 4 MPa) that constitute the machine stabilization phase of loading (as mentioned in Section 4.2.2). The evolution of true stress amplitude of all

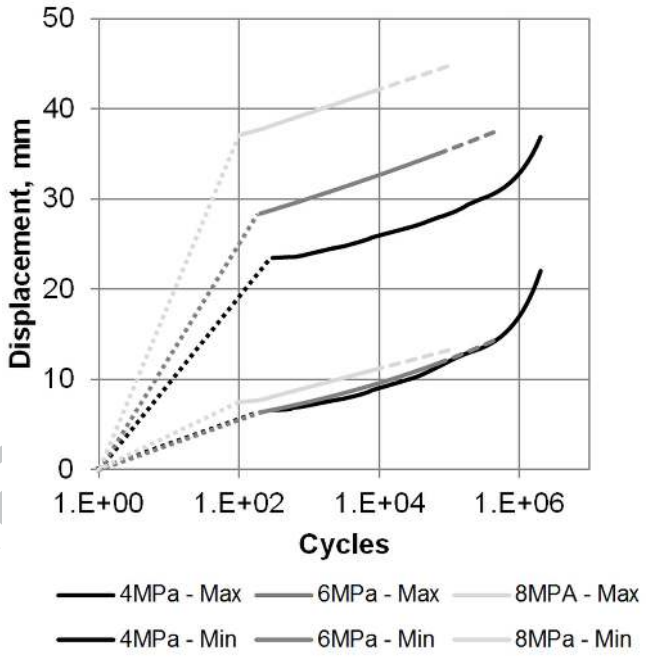

Figure 13: Master curves for prescribed constant true stress amplitude of 4, 6, and 8 MPa and R=0.

tested specimens for each loading level are shown in Figure 14. Tables 1 to 3 show for each loading level and specimen: the average stress amplitude over the duration of the fatigue life; percent difference of the average stress amplitude with respect to the target stress amplitude; and, the stress range defined as the difference between the maximum and the minimum values of true stress amplitude measured. For all loading levels, it appears that the actual stress amplitude experienced by each specimen is not exactly equivalent to the target stress as indicated by the percent difference. This phenomenon could be explained by the fact that during specimen installation (although extra precaution has

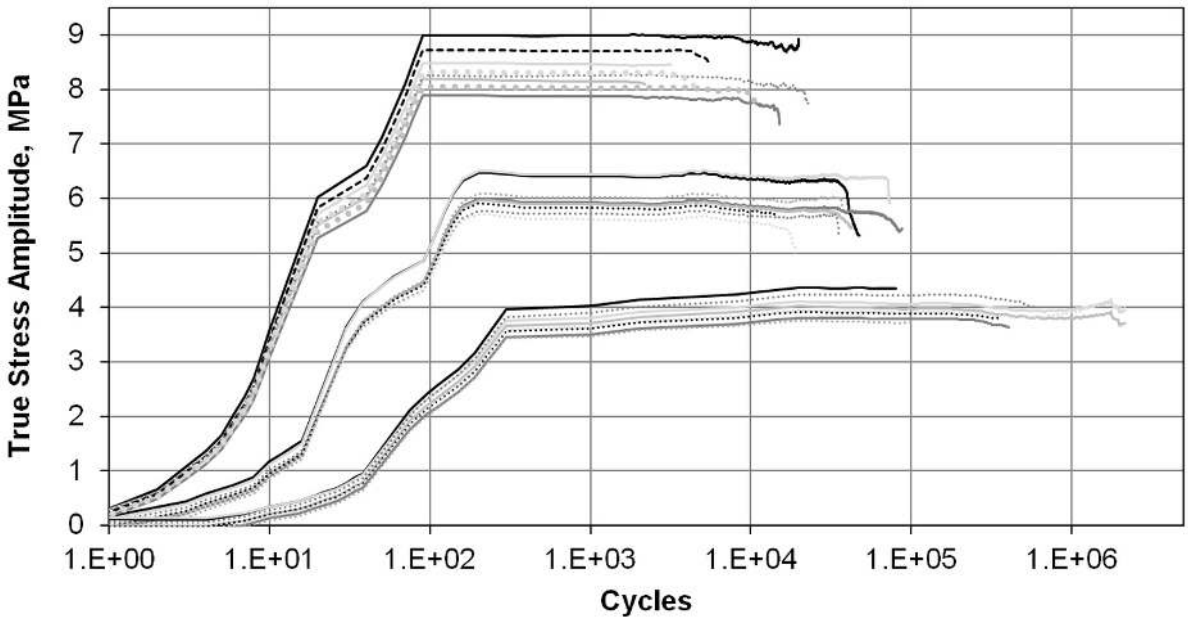

Figure 14: Evolution of true stress amplitude under parallel loading of 4, 6, and 8 MPa.

been taken) each specimen is slightly in compression or in tension with respect to each other. Moreover, the true stress measured for each specimen is generally not constant as indicated by the stress range. In some cases, such as for two specimens tested at 6 MPa, cracks occur within the specimen that leads to a significant decrease in the measured force - and subsequently of calculated stress; however, this stress value is not the true stress, as the effective cross-section area of the specimen is unknown due to the presence of such cracks. Overall, the magnitudes are deemed to be acceptable in general and the goal for constant true stress amplitude is achieved. Additionally, the actual average R-ratio values are zero $\pm$ 0.01 for all carried out tests.

Table 1: Average stress amplitude, percent difference, and stress range of each specimen tested in parallel at 8MPa.

Specimen	Average Stress Amplitude (MPa)	Percent Difference (%)	Range (±MPa)
1	8.76	9.55	0.12
2	7.82	-2.26	0.04
3	8.23	2.88	0.08
4	8.30	3.76	0.01
5	8.63	7.91	0.03
6	8.05	0.61	0.34
7	8.06	0.81	0.07
8	8.28	3.45	0.01

Table 2: Average stress amplitude, percent difference, and stress range of each specimen tested in parallel at 6MPa.

Specimen	Average Stress Amplitude (MPa)	Percent Difference (%)	Range (±MPa)
1	5.98	-0.35	0.52
2	5.76	-3.96	0.24
3	5.74	-4.36	0.18
4	6.19	3.19	0.13
5	5.76	-3.95	0.04
6	5.58	-6.93	0.00
7	6.08	1.39	0.01
8	5.58	-7.04	0.20

Table 3: Average stress amplitude, percent difference, and stress range of each specimen tested in parallel at 4MPa.

Specimen	Average Stress Amplitude (MPa)	Percent Difference (%)	Range (±MPa)
1	4.25	6.31	0.03
2	3.82	-4.50	0.04
3	3.79	-5.25	0.15
4	3.78	-5.39	0.07
5	3.76	-6.02	0.05
6	3.93	-1.74	0.06
7	3.86	-3.47	0.02
8	3.86	-3.53	0.05

4.4 Wöhler curve

Finally, the primary objective of plotting of a Wöhler curve, showing the fatigue life results for the tested elastomer, is achieved as presented in Figure 15. Here, the average true stress of an individual specimen is plotted with respect to the number of cycles to failure (experiments were stopped at around 2 million cycles for 3 specimens at target amplitude of 4 MPa). Since, for both individual and parallel testing, the actual true stress experienced by the material is measured, the present procedure allows to plot the exact loading experienced by each specimen, which is useful for a future extensive statistical analysis.

5 Conclusion

Conventional fatigue life testing, where loading is prescribed in displacement, is not appropriate for materials exhibiting strong inelastic behavior: mechanical (stress and strain) parameters are not constant and a proper Wöhler curve cannot be constructed. A procedure for testing in true stress control is developed. Tests in true stress control allow to keep at least one mechanical state parameter constant; thereby, it allows to make valid comparisons between different materials and predictions in design. First, the area is esti-

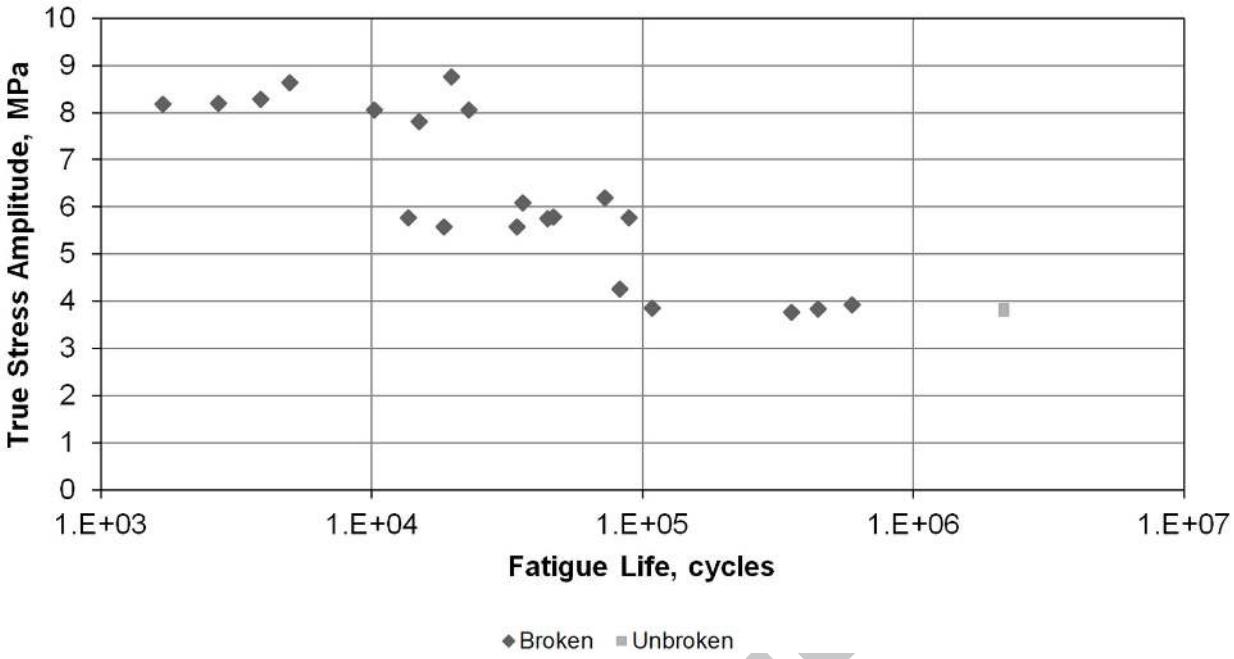

Figure 15: Wöhler curve of HNBR, R=0.

mated by digital image correlation measurements and finite element analysis as a function of prescribed displacement. Afterwards, a machine algorithm allows reaching a constant true stress target during testing of a single specimen. The procedure can also be extended to parallel testing by creation of master displacement curves; the master curves contain the minimum and maximum prescribed displacement values for a specific loading level as a function of number of cycles. Finally, the master curves are used to carry out tests on multiple specimens in parallel using a special experimental setup.

First results show that the procedure accurately calculates and maintains the prescribed true stress targets. In individual testing, good repeatability is observed for different specimens tested at same loading levels. In parallel testing, the amplitude is almost constant as desired; however, the target stress amplitude cannot be reached for all specimens when tested in parallel, as each is under slightly different loading conditions at the start of the experiments. It appears that these errors are not procedure specific, but related to the experimental setup and the utilized equipment. Careful consideration has to be made with respect to the installation of specimens in eliminating these errors. Finally, we can state that a relevant Wöhler curve is plotted, which can be further used with application of some fatigue criteria.

6 Acknowledgments

We would like to thank Ivanna Pivdiablyk for carrying out the initial experiments as part of her Master thesis and to James Cooke of Instron for assistance with the machine software. Additionally, we would like to express our sincere gratitude to the Reviewers for their insightful comments that helped to improve the clarity of this article.

References

[1] W. Mars and A. Fatemi, "A literature survey on fatigue analysis approaches for rubber," *International Journal of Fatigue*, vol. 24, no. 9, pp. 949–961, 2002.

[2] S. Svensson, "Testing methods for fatigue properties of rubber materials and vibration isolators," *Polymer Testing*, vol. 2, no. 3, pp. 161–174, 1981.

[3] ASTM International, "ASTM D4482 - 99: Standard Test Method for Rubber Property-Extension Cycling Fatigue," 1999.

[4] W. Schütz, "A history of fatigue," *Engineering Fracture Mechanics*, vol. 54, no. 2, pp. 263–300, 1996.

[5] P. Forrest, *Fatigue of metals*. Elsevier, 2013.

[6] R. I. Stephens and H. O. Fuchs, *Metal fatigue in engineering*. Wiley, 2001.

[7] S. M. Cadwell, R. A. Merrill, C. M. Sloman, and F. L. Yost, "Dynamic Fatigue Life of Rubber," *Industrial & Engineering Chemistry Analytical Edition*, vol. 12, no. 1, pp. 19–23, 1940.

[8] J. H. Fielding, "Flex life and crystallization of synthetic rubber," *Industrial and Engineering Chemistry*, vol. 35, no. 12, pp. 1259–1261, 1943.

[9] J. R. Beatty, "Fatigue of Rubber," *Rubber Chemistry and Technology*, vol. 37, no. 5, pp. 1341–1364, 1964.

[10] W. V. Mars and W. Vernon, *Multiaxial fatigue of rubber*. ProQuest LLC, 2001.

[11] E. Verron and A. Andriyana, "Definition of a new predictor for multiaxial fatigue crack nucleation in rubber," *Journal of the Mechanics and Physics of Solids*, vol. 56, pp. 417–443, feb 2008.

[12] N. Saintier, G. Cailletaud, and R. Piques, "Multiaxial fatigue life prediction for a natural rubber," *International Journal of Fatigue*, vol. 28, no. 5, pp. 530–539, 2006.

[13] W. V. Mars and A. Fatemi, "Fatigue crack nucleation and growth in filled natural rubber," *Fatigue and Fracture of Engineering Materials and Structures*, vol. 26, no. 9, pp. 779–789, 2003.

[14] E. M. Arruda and M. C. Boyce, "A three-dimensional constitutive model for the large stretch behavior of rubber elastic materials," *Journal of the Mechanics and Physics of Solids*, vol. 41, no. 2, pp. 389–412, 1993.

[15] J. S. Bergström and M. C. Boyce, "Constitutive modeling of the large strain time-dependent behavior of elastomers," *Journal of the Mechanics and Physics of Solids*, vol. 46, no. 5, pp. 931–954, 1998.

[16] W. V. Mars and A. Fatemi, "Factors that affect the fatigue life of rubber: a litterature survey," *Rubber Chemistry and Technology*, vol. 77, no. 3, pp. 391–412, 2004.

[17] J. Diani, B. Fayolle, and P. Gilormini, "A review on the Mullins effect," *European Polymer Journal*, vol. 45, no. 3, pp. 601–612, 2009.

[18] G. Chagnon, E. Verron, L. Gornet, G. Marckmann, and P. Charrier, "On the relevance of Continuum Damage Mechanics as applied to the Mullins effect in elastomers," *Journal of the Mechanics and Physics of Solids*, vol. 52, no. 7, pp. 1627–1650, 2004.

[19] C. J. Derham and A. G. Thomas, "Creep of Rubber under Repeated Stressing," *Rubber Chemistry and Technology*, vol. 50, pp. 397–402, may 1977.

[20] J. G. R. Kingston and A. H. Muhr, "Effects of Strain Crystallisation on Cyclic Fatigue of Rubber," *6th Engineering Integrity Society International Conference on Durability and Fatigue*, 2007.

[21] W. V. Mars and A. Fatemi, "Observations of the Constitutive Response and Characterization of Filled Natural Rubber Under Monotonic and Cyclic Multiaxial Stress States," *Journal of Engineering Materials and Technology*, vol. 126, no. 1, p. 19, 2004.

[22] W. V. Mars, "Fatigue Life Prediction for Elastomeric Structures," *Rubber Chemistry and Technology*, vol. 80, no. 3, pp. 481–503, 2007.

[23] S. Asare, A. G. Thomas, and J. J. C. Busfield, "Cyclic Stress Relaxation (Csr) of Filled Rubber and Rubber Components," *Rubber Chemistry and Technology*, vol. 82, pp. 104–112, mar 2009.

[24] G. Ayoub, F. Zaïri, M. Naït-Abdelaziz, J. Gloaguen, and G. Kridli, "A visco-hyperelastic damage model for cyclic stress-softening, hysteresis and permanent set in rubber using the network alteration theory," *International Journal of Plasticity*, vol. 54, pp. 19–33, 2014.

[25] A. Zine, N. Benseddiq, M. Nait Andelaziz, N. Ait Hocine, and D. Bouami, "Prediction of rubber fatigue life under multiaxial loading," *Fatigue & Fracture of Engineering Materials & Structures*, vol. 29, no. 3, pp. 267–278, 2006.

[26] P.-Y. Le Gac, M. Arhant, P. Davies, and A. Muhr, "Fatigue behavior of natural rubber in marine environment: Comparison between air and sea water," *Materials & Design*, vol. 65, pp. 462–467, 2015.

[27] K. Narynbek Ulu, B. Huneau, P.-Y. Le Gac, and E. Verron, "Fatigue resistance of natural rubber in seawater with comparison to air," *International Journal of Fatigue*, vol. 88, pp. 247–256, jul 2016.

[28] N. André, G. Cailletaud, and R. Piques, "Haigh diagram for fatigue crack initiation prediction of natural rubber components," *KGK-Kautschuk und Gummi Kunststoffe*, vol. 52, no. 2, pp. 120–123, 1999.

[29] H. Ismail and R. Jaffri, "Physico-mechanical properties of oil palm wood flour filled natural rubber composites," *Polymer Testing*, vol. 18, no. 5, pp. 381–388, 1999.

[30] J.-H. Kim and H.-Y. Jeong, "A study on the material properties and fatigue life of natural rubber with different carbon blacks," *International Journal of Fatigue*, vol. 27, no. 3, pp. 263–272, 2005.

[31] B. Wang, H. Lu, and G.-h. Kim, "A damage model for the fatigue life of elastomeric materials," *Mechanics of Materials*, vol. 34, no. 8, pp. 475–483, 2002.

[32] K. Legorju-Jago and C. Bathias, "Fatigue initiation and propagation in natural and synthetic rubbers," *International Journal of Fatigue*, vol. 24, no. 2-4, pp. 85–92, 2002.

[33] B. Huneau, "Strain-Induced Crystallization of Natural Rubber: a Review of X-Ray Diffraction Investigations," *Rubber Chemistry and Technology*, vol. 84, no. 3, pp. 425–452, 2011.

[34] S. Beurrot-Borgarino, B. Huneau, E. Verron, and P. Rublon, "Strain-induced crystallization of carbon black-filled natural rubber during fatigue measured by in situ

synchrotron X-ray diffraction," *International Journal of Fatigue*, vol. 47, pp. 1–7, 2013.

[35] N. Saintier, G. Cailletaud, and R. Piques, "Cyclic loadings and crystallization of natural rubber: An explanation of fatigue crack propagation reinforcement under a positive loading ratio," *Materials Science and Engineering A*, vol. 528, no. 3, pp. 1078–1086, 2011.

[36] S. Rausch, M. Ruderer, W. Enke, A. Narváez, M. Ludwig, and T. Alshuth, "Lifetime prediction of elastomer components within gasoline engines," in *Constitutive Models for Rubbers IX*, pp. 363–366, CRC Press, jul 2015.

[37] D. J. Charlton, J. Yang, and K. K. Teh, "A Review of Methods to Characterize Rubber Elastic Behavior for Use in Finite Element Analysis," *Rubber Chemistry and Technology*, vol. 67, pp. 481–503, jul 1994.

[38] I. Raoult, "Structures elastomeres sous chargement cyclique : comportement, fatigue, duree de vie," *PhD Thesis: Ecole Polytechnique X*, 2010.

[39] J. Royo, "Fatigue testing of rubber materials and articles," *Polymer Testing*, vol. 11, pp. 325–344, jan 1992.

[40] M. Johnson, R. Ekins, N. Murphy, S. Jerrams, and J. Hanley, "The Equi-Biaxial Fatigue Characteristics of EPDM under True (Cauchy) Stress Control Conditions," *ECCMR (VIII)*, 2013.